Energy localization in an atomic chain with a topological soliton

L. Timm,[1,*] H. Weimer,[1] L. Santos,[1] and T. E. Mehlstäubler[2]
[1]*Institut für Theoretische Physik, Leibniz Universität Hannover, 30167 Hannover, Germany*
[2]*Physikalisch-Technische Bundesanstalt, 38116 Braunschweig, Germany*

(Received 16 October 2019; accepted 14 July 2020; published 5 August 2020)

Topological defects in low-dimensional nonlinear systems feature a sliding-to-pinning transition of relevance for a variety of scenarios, ranging from biophysics to nano- and solid-state physics. We find that the dynamics after a local excitation results in a highly nontrivial energy transport in the presence of a topological defect, characterized by a strongly enhanced energy localization in the pinning regime. Moreover, we show that the energy flux in ion crystals with a defect can be sensitively regulated by experimentally accessible environmental parameters. Whereas nonlinear resonances can cause an enhanced long-time energy delocalization, robust energy localization persists for distinct parameter ranges, even for long evolution times and large local excitations.

DOI: 10.1103/PhysRevResearch.2.033198

I. INTRODUCTION

Energy transport in low-dimensional systems has attracted sustained attention since the well-known results of Fermi, Pasta, and Ulam in 1955 [1], which showed that ergodicity and thermalization are not inherent in anharmonic particle lattices. Subsequently, several low-dimensional lattice models have been employed to study microscopic energy transport [2–4]. The underlying dynamics of nonlinear many-body systems can exemplarily be investigated by the Frenkel-Kontorova (FK) model [5,6], a ubiquitous and paradigmatic model of nanofriction, which finds applications in a wide range of fields, from condensed matter physics [7–11] to biophysics [12–15]. Only recently have such atomistic systems become experimentally accessible [16–18]. The FK model describes a one-dimensional (1D) particle lattice with harmonic interactions placed into a periodic substrate potential. When the period of the potential is incommensurable to the particle distances it features a transition from a sliding phase (with superlubricity) to a pinned phase, first described by Aubry [19].

Trapped ions constitute an excellent system to probe energy transport with atomic resolution in arbitrary dimensions in both the classical and quantum regimes [20–22]. Recent theoretical works have shown that nontrivial transport features persist in one- and two-dimensional ion Coulomb crystals [23,24]. First measurements have also monitored the time-resolved dynamics of an ion chain after a local excitation, revealing energy transport from one chain end to the other [25,26]. The nonlinearities of the Coulomb interaction become important when topological defects (kinks) are induced into the system [17,27–30]. Kinks may be created by a quench across the structural phase transition from a one-dimensional to a two-dimensional crystal due to the Kibble-Zurek mechanism [28,31]. The precise control of the kink via external trap parameters made it possible to investigate their properties [32,33].

An example for the use of the good control of kinks in trapped ion systems is the study of nanofriction in the FK model. Its original form may be emulated by superimposing an optical lattice to an ion chain [34]; however, the same signatures of Aubry physics have been observed in a self-assembled and back-acting, two-dimensional crystal with a defect [17]. In the latter case the defect introduces the necessary incommensurability. Experiments on both approaches showed the occurrence of reduced friction and a structural symmetry breaking at the Aubry transition [19]. Other efforts have been made to investigate the transport properties of solitonic excitations [6,35–38].

In this paper, we show that energy transport after a local ion displacement [25,26] shows a tunable, highly nontrivial excitation dynamics in the presence of a topological defect of the crystal. Whereas the defect remains transparent to energy flux within the sliding regime, the slight change in the crystal geometry that accompanies the sliding-to-pinning transition results in a very strong enhancement of energy localization. Moreover, nonlinearity results in a complex dependence of the long-time dynamics on the aspect ratio of the trap. Whereas nonlinear resonances enhance delocalization for certain aspect ratios, slightly altered values lead to surprisingly robust energy localization for very long times and large initial ion displacements. Our results reveal the crucial role played by defects in the transport properties, and eventually in the thermalization dynamics and heat conductivity, of self-assembled atomic chains.

II. MODEL

We consider a two-dimensional system consisting of N ions places into a harmonic trapping potential. The ions obey

*lars.timm@itp.uni-hannover.de

the Hamiltonian:

$$H = \sum_i \frac{\vec{p}_i^2}{2m} + V(\{\vec{r}_i\}), \tag{1}$$

where $\vec{p}_i = (p_i^x, p_i^z)$ and $\vec{r}_i = (x_i, z_i)$ are the momentum and the position of the ith ion and m the ion mass. The ions experience a potential that results from the external trap and the Coulomb interaction:

$$V(\{\vec{r}_i\}) = \sum_i \frac{m\omega_z^2}{2}(z_i^2 + \alpha^2 x_i^2) + \frac{1}{2}\sum_{i,j\neq i} \frac{e^2}{4\pi\epsilon_0}\frac{1}{|\vec{r}_{ij}|}, \tag{2}$$

with $\vec{r}_{ij} = \vec{r}_i - \vec{r}_j$, e the elementary charge, ϵ_0 the vacuum permittivity, ω_z the trap frequency along z, and $\alpha = \omega_x/\omega_z$ the trap aspect ratio. We assume that effects due to fast-rotating parts of the trap potential are negligeable. In our simulations we consider a typical experimental scenario with $N = 30$ $^{172}Yb^+$ ions and fixed $\omega_z/2\pi = 25$ kHz. This leaves the ratio of the trapping frequencies α as the only external control parameter.

At equilibrium the ions are located at positions $\vec{r}_{i,0}$, which minimize H and are therefore dependent on α. For $\alpha > \alpha_{ZZ,L}$ ($= 11.98$ in our case) the ions align in a 1D chain along the z axis due to the strong confinement in x. Below that value a two-dimensional zigzag phase (ZZ) develops at the chain center [39]. For $\alpha < \alpha_K$ ($= 9.1$ in our case) a kink inside the zigzag region can be stabilized, forming a solitonic excitation of the zigzag crystal. We constrain our analysis to $\alpha < \alpha_K$, since we are interested in the energy transport in the presence of a kink. In our numerical simulations, we realize an equilibrium arrangement with a topological defect by flipping one half of a zigzag crystal horizontally, e.g., transforming $x_i \to -x_i$ for all ions i with $z_i > 0$, and let the kink find its equilibrium under high damping.

The shape and the dynamics of the kink are determined by an effective kink potential, the Peierls-Nabarro (PN) potential. For $\alpha < \alpha_{SP}$ ($= 6.4$ in our case) is in the so-called sliding (S) phase for which the PN potential globally confines the soliton in the trap center. The ion crystal has therefore mirror symmetry in z [see Fig. 1(b)]. At α_{SP} the kink undergoes an Aubry-type transition to a pinning (P) phase. At this critical value the kink potential is modulated by periodic barriers. In particular, a barrier rises in the trap center so that the kinks new equilibrium position (given by a potential minimum) is forced off the symmetry axis. The crystal symmetry is spontaneously broken as seen in Fig. 1(c). At α_{PO} ($= 7.7$ in our case) the kink undergoes a crossover to the odd (O) phase, in which the radial trapping is sufficiently strong to force a kink ion between the upper ($x_i > 0$) and the lower ($x_i > 0$) subchains that formed the zigzag arrangement [Fig. 1(d)] [28]. The form of the PN potential is changed toward a globally unstable form, still modulated by the periodic barriers, which stabilize the defect by supplying local potential minima. At α_K these local minima become too shallow, and the soliton slips out of the crystal and is lost.

As shown below, both the S-to-P transition and the crossover into the O phase has dramatic consequences for the transport and localization of excitations in the crystal, even if the change in the crystal structure is minimal (as it is particularly the case at the S-to-P transition).

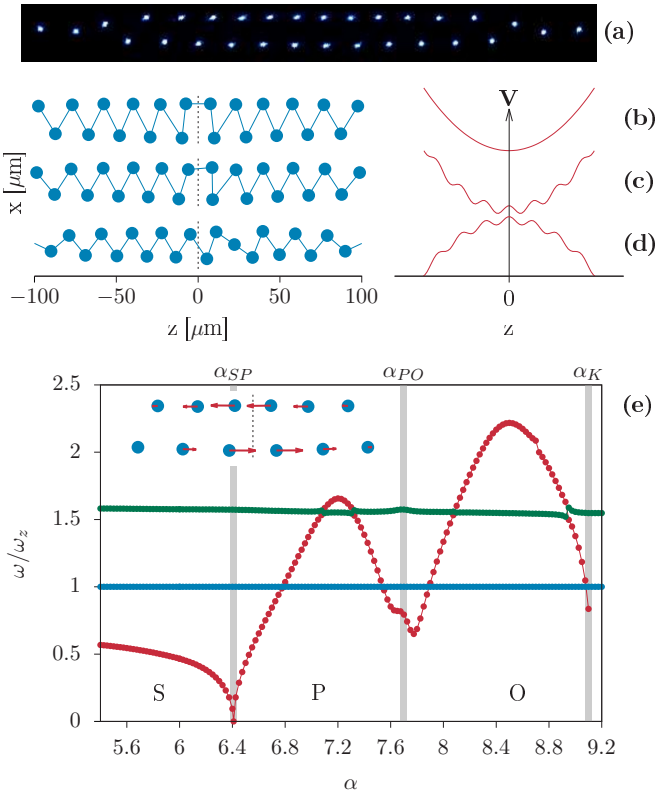

FIG. 1. (a) Photo of an ion crystal with a central zigzag region with a kink in the sliding (S) phase, experimental picture from Ref. [40]. Computed equilibrium positions for the S phase (b), pinned (P) phase (c), and odd-kink (O) regime (d). On the right of the crystal the respective Peierls-Nabarro potential of the kink is schematically depicted. (e) α dependence of the frequency of the kink mode (red) and other low-lying modes. The mode vector of the kink mode is shown in the inset.

III. HARMONIC APPROXIMATION

In harmonic approximation, one considers small deviations of the ions from their equilibrium positions and obtains an effective Hamiltonian after linearization. Whereas for a linear ion chain axial and transversal degrees of freedom decouple, the analysis is significantly more complicated in a zigzag crystal due to the strong coupling between both degrees of freedom. In the following, we discuss how the harmonic approximation is obtained for this more complicated case.

We assume a small deviation $d\vec{r}_i = (dx_i, dz_i) = \vec{r}_i - \vec{r}_{i,0}$ of the ions with respect to their equilibrium positions $\vec{r}_{i,0}$, discussed in the previous part. Expanding the potential (2) up to second order in the deviations we obtain

$$V(\{\vec{r}_i\}) - V(\{\vec{r}_{i0}\}) \simeq \sum_i U_i - \sum_{i,j\neq i} h_{ij}. \tag{3}$$

The potential is given by the sum of a local potential U_i for each ion and their interaction h_{ij}, coming from the Couloumb potential. The coupling of the ions in harmonic approximation

is expressed as

$$h_{ij} = d\vec{r}_i{}^T \underbrace{\begin{pmatrix} W_{ij}^{xx} & W_{ij}^{zx} \\ W_{ij}^{zx} & W_{ij}^{zz} \end{pmatrix}}_{W_{ij}} d\vec{r}_j \tag{4}$$

with

$$W_{ij} = \frac{e^2}{8\pi\epsilon_0 |\vec{r}_{ij,0}|^5} \begin{pmatrix} 2x_{ij,0}^2 - z_{ij,0}^2 & 3z_{ij,0}x_{ij,0} \\ 3z_{ij,0}x_{ij,0} & 2z_{ij,0}^2 - x_{ij,0}^2 \end{pmatrix}. \tag{5}$$

Here $\vec{r}_{ij,0} = (x_{ij,0}, z_{ij,0}) = \vec{r}_{i,0} - \vec{r}_{j,0}$ denotes the ion distances in the equilibrium. Note that in the inhomogeneous linear-zigzag geometry the off-diagonal coefficients W_{ij}^{xz} are generally nonzero. As a result, the x and z degrees of freedom are coupled.

The local potential U_i experienced by the ion i is given by:

$$U_i = \frac{m}{2}\left(\omega_{i,z}^2 dz_i^2 + \omega_{i,x}^2 dx_i^2 + 2\Omega_i^2 dz_i dx_i\right) \tag{6}$$

with

$$\begin{aligned} \omega_{i,x}^2 &= \omega_z^2\alpha^2 + \frac{2}{m}\sum_{j\neq i} W_{ij}^{xx}, \\ \omega_{i,z}^2 &= \omega_z^2 + \frac{2}{m}\sum_{j\neq i} W_{ij}^{zz}, \\ \Omega_i^2 &= \frac{2}{m}\sum_{j\neq i} W_{ij}^{xz}. \end{aligned} \tag{7}$$

Note again that in the local potential there is a coupling between oscillations along x and z via Ω_i. Hence, the eigenaxes that characterize the local harmonic oscillator for each ion are not x or z. Instead, due to the Coulomb interaction and the inhomogeneity of the crystal geometry, the local eigenaxes and eigenfrequencies vary nontrivially with the ion index. We introduce the vibron degrees of freedom $\vec{X}_i = (X_{i,-}, X_{i,+})$ that diagonalize the local potential via local rotations S_i, such that

$$d\vec{r}_i = S_i\vec{X}_i \quad \text{with} \quad S_i = \begin{pmatrix} \cos\phi_i & \sin\phi_i \\ -\sin\phi_i & \cos\phi_i \end{pmatrix}. \tag{8}$$

Inserting this ansatz into the local potential of Eq. (6) and solving for vanishing off-diagonal terms gives the local rotation angles ϕ_i and the vibron frequencies $\Lambda_{i,\mu}$:

$$\begin{aligned} \tan 2\phi_i &= \frac{2\Omega_i^2}{\omega_{i,z}^2 - \omega_{i,x}^2}\,\Lambda_{i,\mu}^2 \\ &= \frac{\omega_{i,x}^2 + \omega_{i,z}^2}{2} \pm \frac{1}{2}\sqrt{\left(\omega_{i,z}^2 - \omega_{i,x}^2\right)^2 + \Omega_i^4}. \end{aligned} \tag{9}$$

Finally, we need to transform the coupling terms h_{ij} into the vibron basis and obtain the harmonic Hamiltonian:

$$H_H = \sum_{i,\sigma=\pm}\frac{P_{i,\sigma}^2}{2m} + \sum_{i,\sigma=\pm}\frac{m}{2}\Lambda_{i,\sigma}^2 X_{i,\sigma}^2 - \frac{1}{2}\sum_{i,\,j\neq i\,\sigma,\sigma'=\pm} \tilde{U}_{ij}^{\sigma\sigma'} X_{i,\sigma}X_{j,\sigma'}. \begin{pmatrix} U_{ij}^{--} & U_{ij}^{-+} \\ U_{ij}^{+-} & U_{ij}^{++} \end{pmatrix} = S_i^T W_{ij} S_j. \tag{10}$$

The diagonalization of H_H provides an alternative picture in terms of phononlike excitations of the crystal.

With each phonon mode oscillating with its respective frequency the excitation dynamics in this picture is given by the group velocity of the modes, describing the dephasing of the mode amplitudes.

In particular, the presence of a kink results in a global mode with strongly localized amplitude at the defect (kink mode), which shows an interesting dependence on α [Fig. 1(e)], vanishing at the S-to-P transition and showing a marked minimum at the onset of the O phase.

IV. ENERGY LOCALIZATION

In our simulations, we first determine the equilibrium positions of the ions for a given $\alpha < \alpha_K$ (we restrict to $\alpha > 5.5$, since for lower α the crystal may undergo a structural transition into a three-layer arrangement). We then perform instantaneously at time $t = 0$ a displacement of a single chosen ion, resulting in a coherent state, which may be experimentally realized as in Ref. [25]. After inducing this local perturbation, the system evolves freely, and its initially localized energy may propagate through the ion crystal. In order to study the resulting dynamics, we solve the Hamilton equations of motion corresponding to Eq. (1), when considering the exact evolution, or of Eq. (10), when restricting to the harmonic approximation. We then characterize the propagation of excitations by monitoring the local kinetic energy $E_i(t) = m\dot{\vec{r}}_i(t)^2/2$ for the i ion at time $t > 0$.

The excitation dynamics is markedly different in the S and in the P phases, as shown in Fig. 2 for the case of an initial displacement of 1 μm of ion 7 along the z direction. Whereas in the S phase the energy can be quickly transported across the system within tens of μs, in the P phase the kink strongly blocks energy transport. The excitation remains localized within one half of the crystal, unable to cross the defect region. The starkly different behavior can be traced back to the spatial amplitude distribution of the phononlike modes that become populated by the initial excitation. Due to the asymmetric crystal the dominant modes are strongly localized in the excited half of the crystal. These modes are unable to transport energy across the defect which leads to an energy blockade.

The observed energy localization is best characterized by the time-averaged kinetic energy (after a time τ) at one half of the crystal, e.g., $E_{\text{left}} = \sum_{z_i<0}\langle E_i\rangle$, with $\langle E_i\rangle = \frac{1}{\tau}\int_0^\tau dt E_i(t)$. We define ΔE as the ratio between E_{left} and the total energy of the system. Mirror symmetric energy distributions are characterized by $\Delta E = 0.5$, whereas localization at the left half results in $\Delta E > 0.5$.

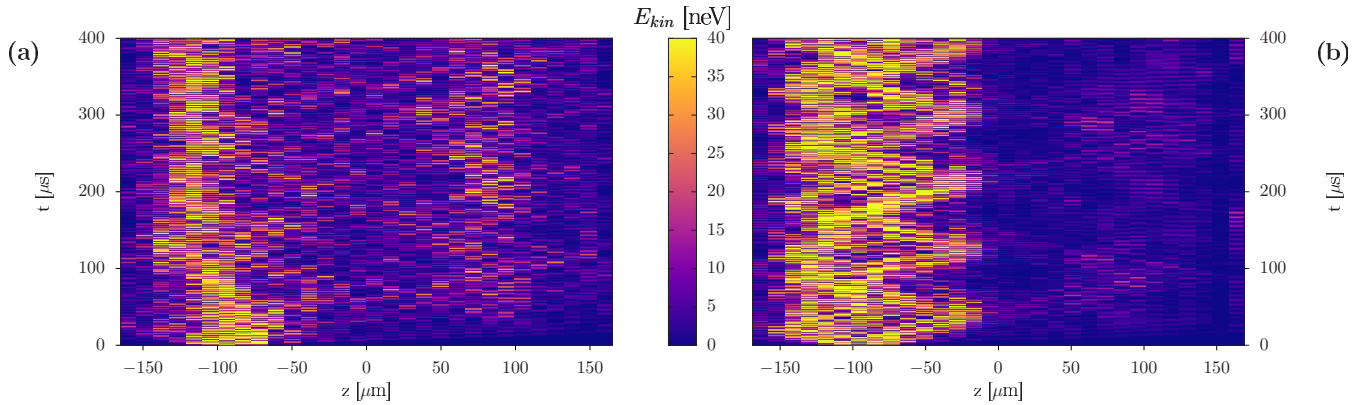

FIG. 2. Dynamics of the kinetic energy after a 1 μm displacement of ion 7 along z, calculated using Eq. (10), for (a) $\alpha = 5.5$ (sliding phase) and (b) $\alpha = 6.8$ (pinning phase).

A. Harmonic transport

Figure 3(a) shows ΔE, for an initial displacement of the leftmost ion by 1 μm along x, averaged over $\tau = 100$ ms (much longer than the dynamics timescale $T_z = 2\pi/\omega_z = 40$ μs). The blue circles depict our results using the Hamiltonian in harmonic approximation of Eq. (10). For $\alpha < \alpha_{SP}$ the energy distribution is mainly symmetric ($\Delta E = 0.5$) due to the transparency of the kink in the S phase. However, for some α values the energy remains localized even in the S phase for a long time, leading to sharp peaks in ΔE. The anomalously slow delocalization results from the crossing of two harmonic modes for certain α values. If these modes are strongly populated by the initial excitation, the mode degeneracy results in very slow dephasing, handicapping delocalization even at long times.

At $\alpha > \alpha_{SP}$, the crystal symmetry is spontaneously broken, leading to an abrupt increase of ΔE, which peaks at $\alpha \simeq 6.8$, for which over 90% of the energy remains localized at the left side. This sensitivity of the transport properties at the S-to-P transition is particularly surprising, considering that the equilibrium geometry is only slightly modified at the transition [see Fig. 1(c)]. Localization is also strongly enhanced at α_{PO} by the appearance of the odd kink, reaching up to a maximal $\Delta E = 0.85$. Finally, at α_K the kink becomes unstable and disappears, and with it the energy localization, resulting in $\Delta E = 0.5$. Although the quantitative values of ΔE depend on the initially excited ion, the amplitude, and the direction of the displacement, similar significant localization is observed at the Aubry-type transition and at the onset of the odd kink for all choices of the initial excitation.

B. Anharmonic transport

Although the harmonic approximation provides useful insights about the dynamics, in particular at short times, the actual energy transport, especially in the long-time limit and for larger displacements, is provided by the Hamilton equations resulting from the Hamiltonian (1). The corresponding results are depicted with red circles in Fig. 3(a). In the sliding phase the dynamics is well described by the harmonic approximation. In the symmetry-broken phases anharmonic effects result in considerable delocalization which compensates the energy imbalance between the left and the right halves. This is particularly so when the PN barriers are small (close to α_{SP} and α_K) so that the excitation may be strong enough to trigger the movement of the kink across the barrier into a neighboring minimum of the PN potential (close to α_K the kink is lost, see Fig. 1). As a result, at those α values the anharmonic effects are particularly strong even for small initial ion displacements.

Interestingly, nonlinear delocalization also occurs deep inside the pinning and odd phase at particular windows of α values. Delocalization on a timescale of hundreds of ms appears in α ranges intertwined with α regions where localization is surprisingly robust and well described by the harmonic approximation even at very long times, well over 100 ms. Figure 3(b), which zooms in the window $6.95 < \alpha < 7.05$, clearly illustrates the dense structure of intertwined harmonic (localized) and anharmonic (delocalized) regions.

The observed anharmonic delocalization of energy for particular α values is due to a third-order resonance of the phononlike modes. It occurs when the frequency ω_{exc} of an eigenmode, localized in one crystal half and strongly populated by the initial excitation, equals the sum of two lower-lying mode frequencies which have a significant amplitude in both crystal halves (see Fig. 4). This leads to a strong coupling between these three eigenmodes, enabling transport across the kink. Our results for different averaging times [Fig. 3(b)] show that anharmonic delocalization occurs in a typical timescale of 10–100 ms. Due to the sensitivity of the nonlinear effects to α the weak micromotion of the ions in an experimental setup, which influences the eigenmode frequencies, might shift the resonant α values. The calculation of this perturbation is, however, out of the scope of this paper.

Larger initial displacements enhance nonlinear effects, leading to a broadening of the anharmonic resonances, as illustrated in Fig. 5, where the observable ΔE is shown for different displacement amplitudes. Within the harmonic windows of α values, the localization is remarkably robust up to very large displacements of 1.5 μm. For stronger displacements the energy brought into the system is large enough to break through the energy blockade for all choices of α. Figure 5 shows as well clear dips at the broadened nonlinear resonances. In the vicinity of the resonance at $\alpha \simeq 7.01$ even tiny displacements result in nonlinear delocalization due to mode coupling.

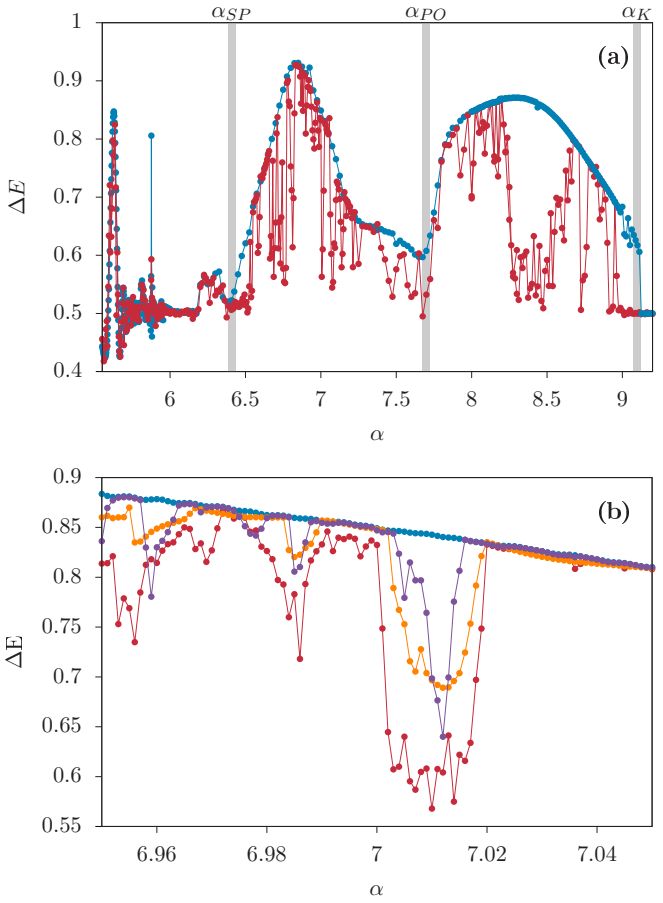

FIG. 3. (a) ΔE as a function of α averaged for $\tau = 100$ ms after an initial displacement of the leftmost ion by 1 μm along x. Blue and red circles indicate, respectively, the results obtained from the harmonic approximation [Eq. (10)] and the exact evolution [Eq. (1)]. (b) Same as (a), zooming in the region $6.95 < \alpha < 7.05$. Red and blue curves depict the same results as (a). The orange curve depicts the results for $\tau = 20$ ms, whereas the purple curve shows ΔE for an initial displacement of 0.5 μm.

V. CONCLUSIONS

Coulomb crystals with a topological defect present a highly nontrivial dynamics. Energy transport of initially localized excitations is remarkably sensitive to the external confinement by two ways. First, changes of the soliton properties (sliding-to-pinning transition, odd-ion crossover) are accompanied by a surprisingly strong energy localization, even if the corresponding change in the crystal geometry is very small. Second, nonlinear effects critically determine the long-time dynamics as a function of the trap aspect ratio. Couplings between phonon modes lead to an intricate structure of windows of resonantly enhanced transport and regimes of surprisingly robust localization even for very long evolution times and large initial displacements.

Although we have focused on ion chains, the discussed transport properties in the presence of a topological defect are relevant as well for other systems (e.g., DNA strains with loop defects [13]) and for other types of repulsive interactions.

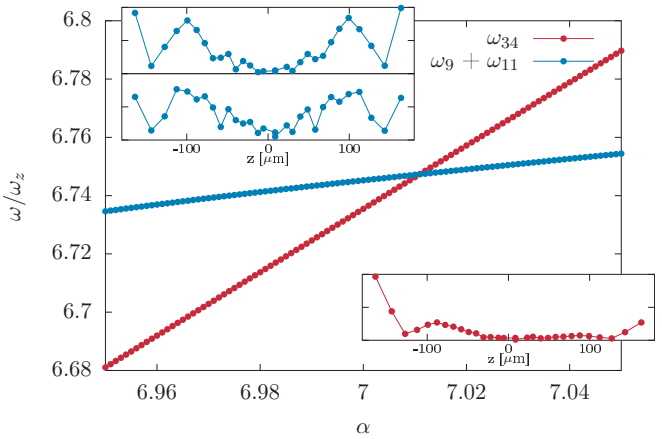

FIG. 4. The mode frequency of the most excited mode by the initial displacement (red) and the sum of two nonexcited modes (blue), as an example for the appearance of nonlinear resonances. The spatial amplitude distribution of the involved modes are shown in the insets. While the excited mode is localized the two low-frequency modes have major contributions in both crystal halves.

Our work shows that energy flux in an atomic chain can be controlled and steered by slight modifications of the defect properties (in our case by very small changes of the trap aspect ratio). Our results are therefore interesting for the engineering of novel cooling techniques and the motional control of ion crystals in experiments dedicated to precision spectroscopy [41–43] and tests of fundamental physics [44,45]. They also emphasize the importance of defects for the exchange of energy between two thermal baths in low-dimensional systems, from solid-state nanosystems to biomolecules like DNA [2,14], and pave the way for future experiments on quantum thermodynamics [21,23,24].

ACKNOWLEDGMENTS

We thank J. Kiethe and H. Fürst for discussions and comments on the manuscript. The authors acknowledge the support from the DFG (Grants No. SFB 1227 DQ-mat,

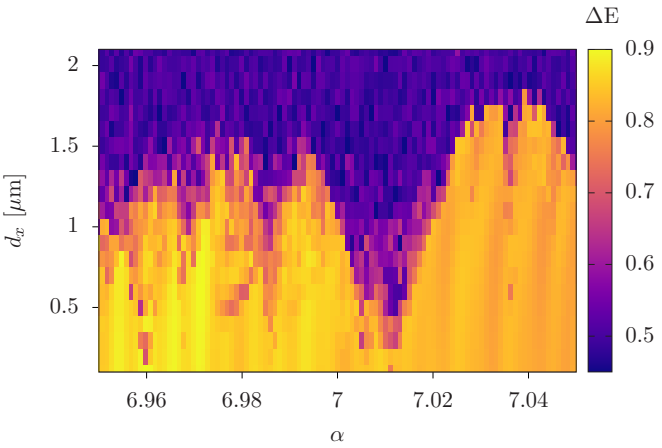

FIG. 5. ΔE for different initial displacement amplitudes d_x of the leftmost ion along x, integrated over $\tau = 100$ ms.

Project A07, and No. EXC 2123 QuantumFrontiers) and the Volkswagen Foundation. This project has received funding from the European Metrology Programme for Innovation and Research (EMPIR) cofinanced by the Participating States and from the European Union's Horizon 2020 research and innovation programme (Project No. 17FUN07 CC4C).

[1] E. Fermi, J. Pasta, and S. Ulam, Los Alamos Report No. LA-1940 (1955).
[2] A. V. Savin and O. V. Gendelman, Phys. Rev. E **67**, 041205 (2003).
[3] S. Lepri, R. Livi, and A. Politi, Phys. Rep. **377**, 1 (2003).
[4] A. Dhar, Adv. Phys. **57**, 457 (2008).
[5] T. Kontorova and Y. I. Frankel, Zh. Eksp. Teor. Fiz. **8**, 1340 (1938).
[6] O. M. Braun and Y. S. Kivshar, *The Frenkel-Kontorova Model: Concepts, Methods, and Applications* (Springer, Berlin, 2004).
[7] T. Brazda, A. Silva, N. Manini, A. Vanossi, R. Guerra, E. Tosatti, and C. Bechinger, Phys. Rev. X **8**, 011050 (2018).
[8] T. Bohlein, J. Mikhael, and C. Bechinger, Nat. Mater. **11**, 126 (2011).
[9] L. Bruschi, A. Carlin, and G. Mistura, Phys. Rev. Lett. **88**, 046105 (2002).
[10] P. Bak, Rep. Prog. Phys. **45**, 587 (1982).
[11] P. M. Chaikin and T. C. Lubensky, Walls, kinks and solitons, in *Principles of Condensed Matter Physics* (Cambridge University Press, Cambridge, 1995), p. 590.
[12] S. W. Englander, N. R. Kallenbach, A. J. Heeger, J. A. Krumhansl, and S. Litwin, Proc. Natl. Acad. Sci. USA **77**, 7222 (1980).
[13] L. V. Yakushevich, *Nonlinear Physics of DNA* (Wiley-VCH, New York, 2004).
[14] F. Kühner, J. Morfill, R. A. Neher, K. Blank, and H. E. Gaub, Biophys. J. **92**, 2491 (2007).
[15] V. Bormuth, V. Varga, J. Howard, and E. Schäffer, Science **325**, 870 (2009).
[16] D. A. Gangloff, A. Bylinskii, and V. Vuletić, Phys. Rev. Res. **2**, 013380 (2020).
[17] J. Kiethe, R. Nigmatullin, D. Kalincev, T. Schmirander, and T. E. Mehlstäubler, Nat. Commun. **8**, 15364 (2017).
[18] M. Dienwiebel, G. S. Verhoeven, N. Pradeep, J. W. M. Frenken, J. A. Heimberg, and H. W. Zandbergen, Phys. Rev. Lett. **92**, 126101 (2004).
[19] S. Aubry, Physica D **7**, 240 (1983).
[20] A. Ruiz, D. Alonso, M. B. Plenio, and A. del Campo, Phys. Rev. B **89**, 214305 (2014).
[21] A. Bermudez, M. Bruderer, and M. B. Plenio, Phys. Rev. Lett. **111**, 040601 (2013).
[22] M. Tamura, T. Mukalyama, and K. Toyoda, Phys. Rev. Lett. **124**, 200501 (2020).
[23] G.-D. Lin and L.-M. Duan, New J. Phys. **13**, 075015 (2011).
[24] N. Freitas, E. A. Martinez, and J. P. Paz, Phys. Scr. **91**, 013007 (2015).
[25] M. Ramm, T. Pruttivarasin, and H. Häffner, New J. Phys. **16**, 063062 (2014).
[26] A. Abdelrahman, O. Khosravani, M. Gessner, A. Buchleitner, H. P. Breuer, D. Gorman, R. Masuda, T. Pruttivarasin, M. Ramm, P. Schindler, and H. Häffner, Nat. Commun. **8**, 15712 (2017).
[27] M. Mielenz, J. Brox, S. Kahra, G. Leschhorn, M. Albert, T. Schaetz, H. Landa, and B. Reznik, Phys. Rev. Lett. **110**, 133004 (2013).
[28] K. Pyka, J. Keller, H. L. Partner, R. Nigmatullin, T. Burgermeister, D. M. Meier, K. Kuhlmann, A. Retzker, M. B. Plenio, W. H. Zurek, A. del Campo, and T. E. Mehlstäubler, Nat. Commun. **4**, 2291 (2013).
[29] S. Ulm, J. Roßnagel, G. Jacob, C. Degünther, S. T. Dawkins, U. G. Poschinger, R. Nigmatullin, A. Retzker, M. B. Plenio, F. Schmidt-Kaler, and K. Singer, Nat. Commun. **4**, 2290 (2013).
[30] S. Ejtemaee and P. C. Haljan, Phys. Rev. A **87**, 051401(R) (2013).
[31] A. del Campo, G. De Chiara, G. Morigi, M. B. Plenio, and A. Retzker, Phys. Rev. Lett. **105**, 075701 (2010).
[32] H. Landa, B. Reznik, J. Brox, M. Mielenz, and T. Schaetz, New J. Phys. **15**, 093003 (2013).
[33] H. L. Partner, R. Nigmatullin, T. Burgermeister, K. Pyka, J. Keller, A. Retzker, M. B. Plenio, and T. E. Mehlstäubler, New J. Phys. **15**, 103013 (2013).
[34] A. Bylinskii, D. Gangloff, I. Counts, and V. Vuletić, Nat. Mater. **15**, 717 (2016).
[35] O. F. Oxtoby and I. V. Barashenkov, Phys. Rev. E **76**, 036603 (2007).
[36] V. Ahufinger, A. Sanpera, P. Pedri, L. Santos, and M. Lewenstein, Phys. Rev. A **69**, 053604 (2004).
[37] J. Abdullaev, D. Poletti, E. A. Ostrovskaya, and Y. S. Kivshar, Phys. Rev. Lett. **105**, 090401 (2010).
[38] J. Brox, P. Kiefer, M. Bujak, T. Schaetz, and H. Landa, Phys. Rev. Lett. **119**, 153602 (2017).
[39] S. Fishman, G. De Chiara, T. Calarco, and G. Morigi, Phys. Rev. B **77**, 064111 (2008).
[40] J. Kiethe, R. Nigmatullin, T. Schmirander, D. Kalincev, and T. E. Mehlstäubler, New J. Phys. **20**, 123017 (2018).
[41] N. Herschbach, K. Pyka, J. Keller, and T. E. Mehlstäubler, Appl. Phys. B **107**, 891 (2012).
[42] K. Arnold, E. Hajiyev, E. Paez, C. H. Lee, M. D. Barrett, and J. Bollinger, Phys. Rev. A **92**, 032108 (2015).
[43] N. Aharon, N. Spethmann, I. D. Leroux, P. O. Schmidt, and A. Retzker, New J. Phys. **21**, 083040 (2019).
[44] C. Sanner, N. Huntemann, R. Lange, C. Tamm, E. Peik, M. S. Safronova, and S. G. Porsev, Nature **567**, 204 (2019).
[45] T. E. Mehlstäubler, G. Grosche, C. Lisdat, P. O. Schmidt, and H. Denker, Rep. Prog. Phys. **81**, 064401 (2018).